processes

MDPI

Article

Application of High-Gradient Magnetic Separation for the Recovery of Super-Paramagnetic Polymer Adsorbent Used in Adsorption and Desorption Processes

Jyi-Yeong Tseng [1], Chia-Chi Chang [1], Cheng-Wen Tu [1], Min-Hao Yuan [2], Ching-Yuan Chang [1,*], Chiung-Fen Chang [3], Yi-Hung Chen [4], Je-Lueng Shie [5], Dar-Ren Ji [1], Bo-Liang Liu [1] and Matthias Franzreb [6]

[1] Graduate Institute of Environmental Engineering, National Taiwan University, Taipei 106, Taiwan
[2] Department of Occupational Safety and Health, China Medical University, Taichung 404, Taiwan
[3] Department of Environmental Science and Engineering, Tung-Hai University, Taichung 407, Taiwan
[4] Department of Chemical Engineering and Biotechnology, National Taipei University of Technology, Taipei 106, Taiwan
[5] Department of Environmental Engineering, National I-Lan University, Yi-Lan 260, Taiwan
[6] Department of Bioengineering and Biosystems, Karlsruhe Institute of Technology, 76344 Eggenstein-Leopoldshafen, Germany
* Correspondence: cychang3@ntu.edu.tw; Tel.: +886-2-23638994

Abstract: This study examined the application of high-gradient magnetic separation (HGMS) for recycling of super-paramagnetic polymer adsorbent (MPA), namely, polyvinyl acetate-iminodiacetic acid. The HGMS can be incorporated with the adsorption and desorption processes (ADPs) with fresh or regenerated desorbed MPAs and exhausted adsorbed MPAs, respectively. This combines the permanent magnet's advantage of low running costs with the easy operation using the solenoid to flush the filter in place. The effects of the inlet concentration of MPA in solution ($C_{LF,i}$) and the fluid velocity (v_0) or volumetric flow rate (Q_{LF}) on the performance of the recovery of MPA via HGMS were assessed. The results indicated that the separation efficiency (η or P_0), breakthrough time (t_B) and exhaustion time (t_E) of HGMS reduce as $C_{LF,i}$, as well as v_0, increases. Further, the filter saturated capture capacity (σ_S) of HGMS also decreases with increasing v_0. The effect of v_0 on t_B proportional to $1/v_0^2$ is more significant than that on σ_S proportional to $1/v_0$. A kinetic model of HGMS shows good agreements for the experimental and predicted breakthrough results, with determination coefficients of 0.985–0.995. The information obtained in this study is useful for the rational design and proper operation of a HGMS system for the recycling and reuse of MPA in ADPs.

Keywords: super-paramagnetic polymer adsorbent (MPA); high-gradient magnetic separation (HGMS); desorbent; adsorption; desorption; permanent magnet

Citation: Tseng, J.-Y.; Chang, C.-C.; Tu, C.-W.; Yuan, M.-H.; Chang, C.-Y.; Chang, C.-F.; Chen, Y.-H.; Shie, J.-L.; Ji, D.-R.; Liu, B.-L.; et al. Application of High-Gradient Magnetic Separation for the Recovery of Super-Paramagnetic Polymer Adsorbent Used in Adsorption and Desorption Processes. *Processes* **2023**, *11*, 965. https://doi.org/10.3390/pr11030965

Academic Editors: Jacek Gebicki, Pawel Sobieszuk and Piotr Rybarczyk

Received: 18 February 2023
Revised: 17 March 2023
Accepted: 19 March 2023
Published: 21 March 2023

1. Introduction

In the past, magnetic separation (MS) was used for magnetic mineral separation in the metallurgical industry [1], the de-ironization of kaolin in the paper industry [2] and pyrite removal in the coal mining industry [3]. Recently, due to the use of magnetic particles as a carrier with the affinity ligand on the surface, MS technology has been widely applied in biochemistry [4], biomedical engineering [5–7] and environmental engineering, including protein purification [8], separation of lactoferrin [9], cell separation [10], immunoassay [11], enzyme immobilization [4], affinity separation [12–16] and waste water treatment [17–24]. MS uses a magnetic driving force to separate magnetic and non-magnetic materials. In order to increase its efficiency, high-gradient magnetic separation (HGMS) technology has been rapidly developed [8,9]. By filling magnetic matrices into

the MS chamber, it can generate a very high magnetic field strength (or magnetic field intensity, H) and gradient with a strong capture ability for magnetic particles.

The motion of magnetic particles in a fluid can generally be controlled by two forces. One is the magnetic force ($F_m = \mu_0 V_p M_p \cdot \nabla H$). The other is the viscous drag force (viscous resistance force) (F_d), which can be obtained by the Stokes equation ($F_d = 3\pi\mu_f d_p v_{p/f}$). In these notations, μ_0 is the magnetic permeability of the vacuum (= $4\pi \times 10^{-7}$ H m^{-1}); V_p (= (1/6) π d_p^3) is the volume of a magnetic particle; d_p is the particle diameter; M_p (= ($\chi_p - \chi_f$) H) is the magnetization of particles; χ_p and χ_f are, respectively, the magnetic susceptibilities of the particle and fluid; H is the magnetic field strength; μ_f is the fluid viscosity; $v_{p/f}$ is the particle velocity relative to the fluid; ∇H is the magnetic field strength gradient at the location of particle. It can be seen from the above equations that the larger the d_p, the stronger the F_m, or the lower the μ_f, the weaker the F_d, resulting in the easier separation of magnetic particles from the fluid. The increase of the H and gradient of H can promote effective separation. The commonly used MS devices can be classified into four types, namely, intermittent [25,26], mobile [10,27,28], high gradient [29–32] and fluidized bed [33,34].

Previous works studied the syntheses of the magnetic polymer adsorbent (MPA) of polyvinyl acetate-iminodiacetic acid (noted as M-PVAC-IDA) and the chemical modification to enhance the affinity of the adsorbent to adsorb copper (II) from an aqueous solution [17,18]. Meanwhile, the adsorption isotherms were set up. In this study, the HGMS was applied for the recycling and reuse of MPA during the adsorption and desorption processes (ADPs). The use of NdFeB (neodymium-iron-boron) magnets in the yoke allows high magnetic inductions, leading to the efficient and fast separation of magnetic adsorbent particles used in ADPs. It may offer the high recycling efficiency of MPA with low operating costs. Another advantage of HGMS is that the non-magnetic impurities can be excluded from MPA during the recovery of MPA. The novel design using a rotary permanent magnet leads to an "on-off" characteristic of the magnetic field in the separation zone. The HGMS of M-PVAC-IDA (denoted as MPA hereafter) was conducted with various inlet concentrations of MPA ($C_{LF,i}$) of 0.94–4.14 g L^{-1} and volumetric flow rates (Q_{LF}) of 0.417–0.833 L min^{-1} (or flow velocities v_0 of 0.866–1.731 m min^{-1}). The corresponding outlet concentrations of MPA ($C_{LF,e}$) were measured. The separation efficiency of MPA (η or P_0), breakthrough time (or effective separation time) (t_B), exhaustion time (or saturation time) (t_E) and filter saturated capture capacity (σ_S) for HGMS were examined and elucidated for different $C_{LF,i}$ and Q_{LF}. In addition, a kinetic model was applied to describe the breakthrough behaviors of the effluent of HGMS and compared with the experimental results.

2. Materials and Methods

2.1. Materials

The MPA (i.e., M-PVAC-IDA) used was synthesized via suspension polymerization using super-paramagnetic Fe_3O_4 gel and specific chemicals. These included the following. Oleic acid, epichlorohydrin, divinylbenzene and vinyl acetate (VAC) were purchased from Aldrich (Sigma-Aldrich Inc., St. Louis, MO, USA). Iminodiacetic acid (IDA) was obtained from Sigma (Sigma-Aldrich Inc., St. Louis, MO, USA). The MPA is nearly non-porous, with an insignificant porosity of 0.003 and a specific area of the external surface of 12.9 m^2 g^{-1}. The density of the MPA is about 1.63 g cm^{-3}. The size of the MPA particles made is about 500 nm to 2 μm and mostly about 1 μm in number. For the details of the synthesis and other properties of MPA, refer to the previous studies [17,18].

2.2. Device

A HGMS incorporated with adsorption and desorption operations is illustrated in Figure 1. A laboratory-type (Steinert HGF-10 1, Cologne, Germany), permanent, magnet-based HGM separator is used for this study. It is a new type of HGMS separator designed using switchable permanent magnets. The separator operates in a cyclic fashion, making it suitable for suspensions with low and moderate concentrations of magnetic particles. The magnetic flux density (B) is 0.3 Tesla. The pole gap is 25 mm, with a pole shoe area of 100 × 80 mm^2. The total weight is 75 kg. The motor power is 0.12 kW.

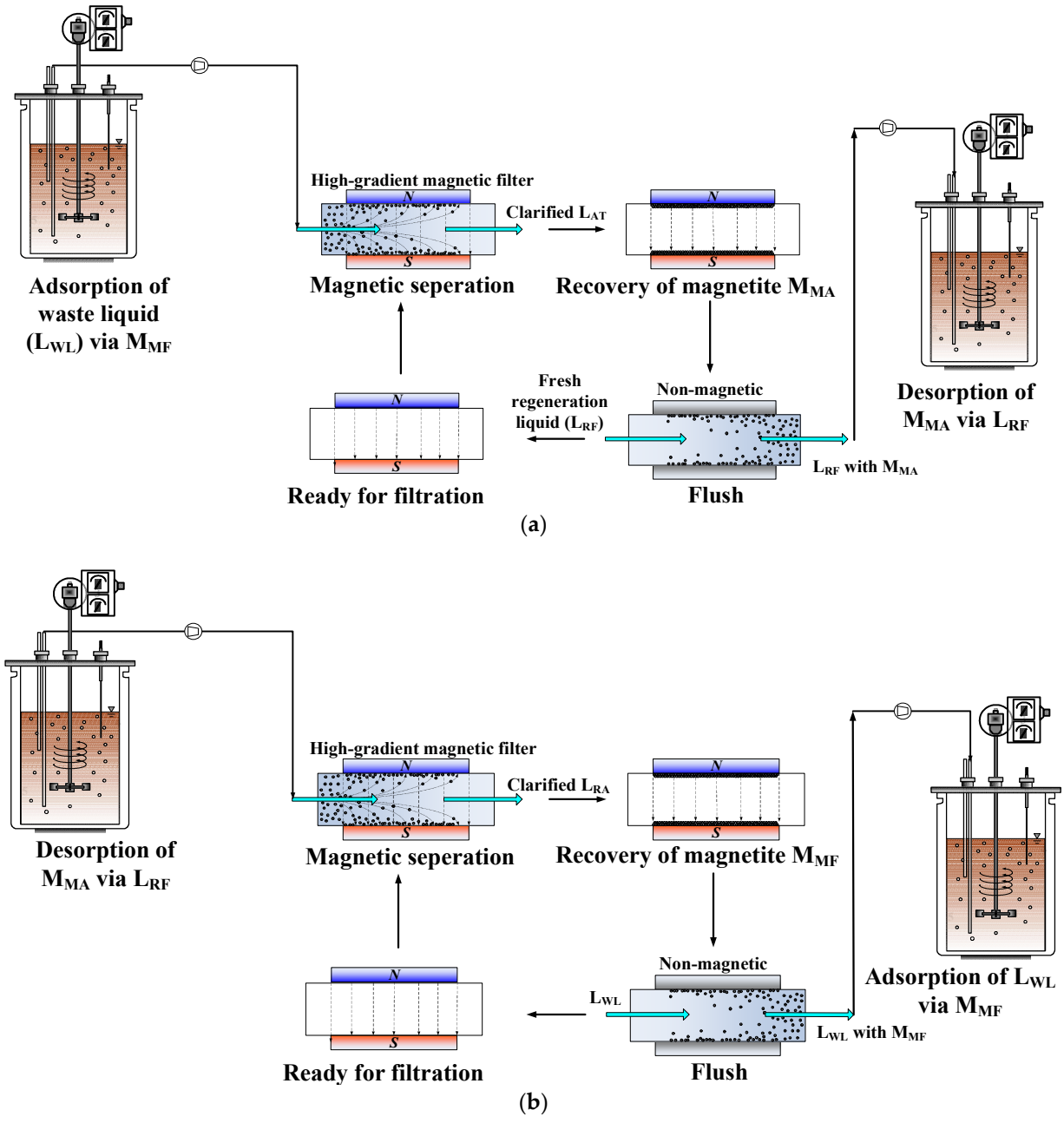

Figure 1. Application of high-gradient magnetic separation (HGMS) incorporated with adsorption and desorption operations. (**a**) Adsorption of waste liquid (L_{WL}) via fresh or freshed (regenerated) magnetite (M_{MF}) and recovery of aged magnetite (M_{MA}); L_{AT}: adsorption treated liquid. (**b**) Desorption/regeneration of M_{MA} via fresh regeneration liquid (L_{RF}) and recovery of freshed (regenerated) magnetite M_{MF}; L_{RA}: aged regeneration liquid.

A filter chamber with size 2.75 × 1.75 × 7.85 cm^3 (volume of filter chamber or cell volume V_c = 37.78 cm^3, height of filter chamber L = 7.85 cm, cell cross-section area A_c = 4.8125 cm^2), containing magnetic matrices, is placed vertically between the poles of the magnet. The matrices are surrounded by a sheet metal housing forming chambers for flow distribution. The matrix filling factor F with all received matrices of mass m_{wm} of 34.5466 g filled in the chamber is 0.1157. The supply and discharge connectors are placed at the ends of the flow distribution chambers. The density of the magnetic wire of the matrix ρ_{wm} is 7900 kg m^{-3}.

2.3. Experimental Conditions

The MPA recovery performance was investigated by monitoring the breakthrough curve of MPA containing fluid. The MPA particles were kept in suspension by continuously mixing the fluid in the batch HGM separator. During operation, the suspension was pumped through the filter chamber until a certain pressure drop was reached or as MPA-containing fluid reached complete breakthrough. After the breakthrough of the MPA, the MPA particles captured by the filter were recovered by a short intensive rinsing in the counter flow direction, with the magnet system switched to "off" until the effluent was clean. Then, the filter chambers were taken out of the magnet system, dismantled and thoroughly cleaned. Finally, the cleaned filter chambers were re-installed, and the magnet was switched to "on" again to start a new filtration cycle.

About 20 g MPA were used to perform the experiments of MS under the following conditions, with various inlet particle concentrations $C_{LF,i}$ and volumetric flow rates Q_{LF}. For the influences of $C_{LF,i}$, the HGMS experiments were conducted at $C_{LF,i}$ of 4.14, 3.21, 2.06, 1.51 and 0.94 g L^{-1} with Q_{LF} of 0.833 L min^{-1}. As for the effects of Q_{LF}, the cases with a Q_{LF} of 0.833, 0.545 and 0.417 L min^{-1}, respectively corresponding to the fluid velocities v_0 of 1.731, 1.132 and 0.866 m min^{-1}, were examined at $C_{LF,i}$ of 2.06 g L^{-1}.

2.4. Analytical Methods

The properties of the MPA were measured by a Superconducting Quantum Interference Device (MPMS7, Quantum Design, Inc., San Diego, CA, USA). The concentration of MPA in liquid was monitored by UV/VIS spectrophotometer (Cintra-20, GBC Scientific Equipment Pty Ltd., Braeside VIC 3195, Australia) at a specific spectrum wave length of 245 nm for assaying the optical density (OD). Additionally, dry weight (DW) measurements were carried out from pooled samples collected during the throughput operation in order to check the relationship of OD/DW via a calibration curve.

2.5. Theoretical Background

2.5.1. Watson and Gerber Theory

There are two ways generally used to describe a HGMS. Firstly, a microscopic level focuses on the forces responsible for the attraction and capture of a single particle on the magnetized wire [35,36]. The other approach uses a macroscopic view, describing the whole filter based on the breakthrough behavior of the filter [37,38].

According to the theory of MS established by Watson [35] and Gerber and Lawson [36], the relationship between the inlet concentration $C_{LF,i}$ and outflow concentration $C_{LF,e}$ of the magnetic particles in the HGM separator can be expressed as the following equation:

$$P = C_{LF,e}/C_{LF,i} = \exp\left[-fFR_{ca}L/(\pi a)\right] \quad (1)$$

In Equation (1), P is the penetration of the magnetic particles in fluid; ($1 - P = \eta$) is the separation efficiency); f is the arrangement factor of magnetic filter media and 4/3 for random filters; F, a and L are the filling factor (or filling density), wire radius and height (or thickness) of magnetic media in the separation chamber, respectively; R_{ca} (= r_c/a) is the dimensionless normalized particle capture radius (r_c). R_{ca} can be expressed as:

$$R_{ca} = (1/2)(v_m/v_0)(a/a_B)^2 \quad (2)$$

where

$$(a_B/a)^4 = (v_m/A_1)t + 1 \quad (3)$$

$$R_{ca} = (1/2)(v_m/v_0)/[(v_m/A_1)t + 1]^{1/2} \quad (4)$$

$$A_1 = [\beta\ \rho_p\ a/(4\ C_{LF,i})] \quad (5)$$

In the above equations, β is the particle aggregation factor with a value of 0.1–0.18; ρ_p is the density of the magnetic particles (kg m^{-3}); v_m is the magnetic velocity (a function of magnetic field strength (H_0) and magnetization of wire of matrix (M_{wm})) (m s^{-1}); v_0 is the flow velocity (m s^{-1}); a_B is the actual wire radius of the magnetic media with the buildup of particles (m); t is the filtration time (also called operation time or separation time) (s).

2.5.2. Mass Balance Approach for Kinetic Models of HGMS

This method is based on a mass balance for the particle suspension carried out over the whole filter volume. For deep-bed filtration, the mass balance of the particles in the MS chamber can be derived and represented with the following equations.

$$(A_c\ dx\ \varepsilon_F)\frac{\partial C}{\partial t} = A_c\ v_0\ C(t,x) - A_c\ v_0\ C(t + dt, x + dx) - \frac{\partial \sigma}{\partial t} A_c\ dx \quad (6)$$

This gives

$$\varepsilon_F \frac{\partial C}{\partial t} = -v_0 \frac{\partial C}{\partial x} - \frac{\partial \sigma}{\partial t} \quad (7)$$

or

$$\varepsilon_F \frac{\partial C}{\partial t} + \frac{\partial \sigma}{\partial t} + v_0 \frac{\partial C}{\partial x} = 0 \quad (8)$$

Assuming $\varepsilon_F \frac{\partial C}{\partial t}$ is negligible compared to the other terms, i.e., $\varepsilon_F \frac{\partial C}{\partial t} \sim 0$, in the dx interval and defining $\tau = t - (\varepsilon_F\ x/v_0)$, Equation (8) can be simplified as Equation (9).

$$\frac{\partial \sigma}{\partial \tau} + v_0 \frac{\partial C}{\partial x} = 0 \quad (9)$$

The time variation of σ increases with v_0, C and the term $\sigma_S - \sigma$, as described below.

$$\frac{\partial \sigma}{\partial \tau} = \lambda\ v_0\ C \quad (10)$$

$$\lambda = \lambda_0\ [1 - (\sigma/\sigma_S)] \quad (11)$$

It can be calculated from Equations (9)–(11) to obtain the solution of the outlet concentration $C_{LF,e}$ as:

$$C_{LF,e}/C_{LF,I} = [\exp(C_{LF,i}\ v_0\lambda_0\tau/\sigma_S)]/([\exp(C_{LF,i}\ v_0\lambda_0\tau/\sigma_S)] + [\exp(\lambda_0 L)] - 1) \quad (12)$$

In the above equations, σ is the capture capacity of a magnetic particle on the magnetic media in a magnetic separation cell at time τ; σ_S is the saturated σ (kg m^{-3}); λ is the characteristic length (m^{-1}); λ_0 is the characteristic length at $\tau = 0$; ε_F is the void fraction of the magnetic matrix; v_0 is the flow velocity (m s^{-1}); A_c is the section area of the separation chamber of the magnetic media (m^2); x and L, respectively, stand for the position at a

certain point in the x direction and the total length of the magnetic media separation chamber (m); C is the concentration at a certain point at the magnetic separation time t (mg L^{-1}); $C_{LF,i}$ and $C_{LF,e}$ are the inflow and outflow concentrations, respectively. The detailed solution of Equation (12) is described in Appendix A.

If the matrix is considered as a single wire, the characteristic length (λ) is related to the capture radius (R_{ca}) and the wire radius of magnetic matrix (a). It can be represented by Equation (11) with Equation (13) as below.

$$\lambda_0 = (2/\pi)\ (1 - \varepsilon_F)\ (R_{ca}/a) \tag{13}$$

2.5.3. Separation Time

Equations (1) and (12) indicate that the penetration of the magnetic particles in the fluid, P, increases with time. The separation time (t_η) at a set separation efficiency η based on Equations (1)–(5) can be obtained as follows.

$$t_\eta = A_1(A_2)^2\ L^2\ (v_m/v_0^2)/\ln(\eta^2) \tag{14}$$

For a given t_η, v_0 must satisfy:

$$v_0 \leqq (A_1)^{1/2}\ A_2\ L\ (v_m/t_\eta)^{1/2}/[\ln(\eta^2)]^{1/2} \tag{15}$$

where

$$A_2 = fF/(2\pi a) \tag{16}$$

$$v_m = 2\mu_0\ (\chi_f - \chi_p)\ M_{wm}\ H_0\ r_p^2/(9\mu_f\ a) \tag{17}$$

In the above equations, H_0 is the magnetic field strength, or the magnetic field intensity (Oe) applied in the x direction perpendicular to the filter; M_{wm} is the magnetization of the wire of the matrix (emu g^{-1} or emu cm^{-3}); r_p is the radius of the paramagnetic particle (μm or nm); μ_f is the viscosity of the fluid ($lb_m\ ft^{-1}$, or kg $m^{-1}s^{-1}$ or N s m^{-2}); μ_0 is the magnetic permeability of the vacuum (= $4\pi \times 10^{-7}$ H m^{-1}); χ_f is the magnetic susceptibility of the fluid (emu cm^{-3} Oe^{-1}); χ_p is the magnetic susceptibility of the particle (emu cm^{-3} Oe^{-1}).

3. Results and Discussion

3.1. Hysteresis Curves of M-PVAC-IDA before and after ADPs

An atom of any substance has its magnetism; therefore, it can be said that all substances are the magnets, and the magnetic extent is dependent on the magnetic strength. Figure 2 shows the comparison of the hysteresis curves of different types of M-PVAC-IDA. The saturation magnetization of Cu(II)-adsorbed M-PVAC-IDA decreases only slightly compared to that of fresh M-PVAC-IDA. Thus, the effect of adsorbed copper on the magnetism of M-PVAC-IDA is insignificant.

However, long-time storage of M-PVAC-IDA resulted in the partial oxidation state of iron and, thus, a significant decline of its saturation magnetization. Figure 2 indicates that the saturation magnetization of M-PVAC-IDA after 2 years of storage time decreased nearly 50%. Therefore, ensuring the preservation of M-PVAC-IDA to maintain its saturation magnetization is an important work for the recycling of ferrite magnetic material or magnetite.

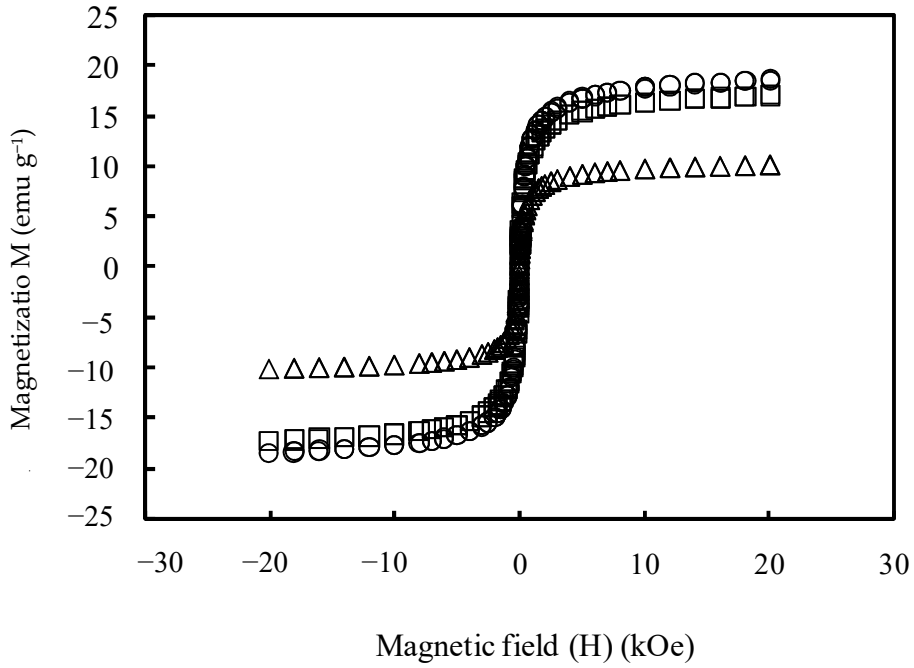

Figure 2. Magnetization curves (*M* vs. *H*) of M-PVAC-IDA particles. ○, □, △: M-PVAC-IDA, Cu(II)-adsorbed M-PVAC-IDA, oxidized M-PVAC-IDA.

3.2. HGMS at Different MPA Concentrations

Figure 3 illustrates the variation of penetration P (= $C_{LF,e}/C_{LF,i}$) with an accumulated volume of liquid filtrated (V_{LF}, expressed as cell volumes (V_c)) at different inlet MPA concentrations $C_{LF,i}$ (4.14, 3.21, 2.06, 1.51 and 0.94 g L^{-1}), with a volumetric flow rate Q_{LF} = 0.833 L min^{-1}. A higher $C_{LF,i}$ shows an easier saturation with a smaller V_{LF}. In the case with the highest $C_{LF,i}$ of 4.14 g L^{-1}, the separation cell reaches P = 95% (denoted as P95), with the smallest V_{LF} of about 70.6 V_c. On the other hand, the lowest $C_{LF,i}$ of 0.94 g L^{-1} gives the largest V_{LF} of about 301.5 V_c at P95. For cases with $C_{LF,i}$ of 1.51, 2.06 and 3.21 g L^{-1}, the corresponding V_{LF} at P95 is 166.7, 131.5 and 90.8 V_c, respectively.

From Equations (2)–(5) of the Watson and Gerber theory, it can be seen that the capture radius R_{ca} is related to the magnetic velocity v_m (thus, the magnetic field strength H_0 and the magnetization of the wire of the matrix M_{wm}, as indicated in Equation (17)), flow velocity v_0, and saturation magnetization M_{Sp} and concentration $C_{LF,i}$ of magnetic particles. When the magnetic field strength and the volumetric flow rate are constant, the actual wire radius a_B of the magnetic media increases, while the capture radius R_{ca} decreases as $C_{LF,i}$ increases. Thus, the saturation of the magnetic particles on the wire of the matrix with a higher concentration will be reached quicker (with a smaller V_{LF}).

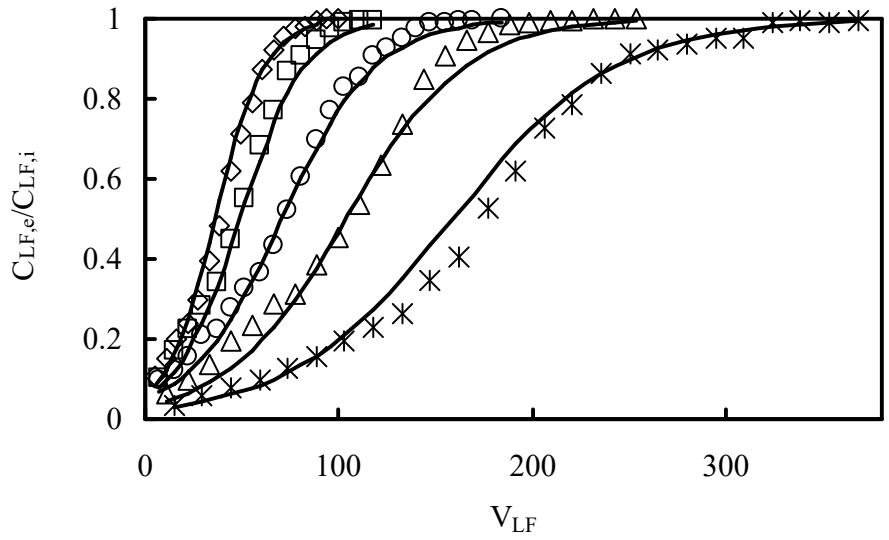

Figure 3. Breakthrough curves for the solution containing M-PVAC-IDA using HGM separator (HGF-10 1) at various $C_{LF,i}$ with Q_{LF} = 0.833 L min^{-1} (v_0 = 1.731 m min^{-1}). ◇, ○, □, △, * : $C_{LF,i}$ = 4.14, 3.21, 2.06, 1.51, 0.94 g L^{-1}. $C_{LF,e}$, $C_{LF,i}$: Outlet and inlet concentrations of M-PVAC-IDA in solution. V_{LF}: Accumulated volume of liquid filtrated expressed as cell volume. Q_{LF}: Volume flow rate. v$_0$: Flow velocity. —: Prediction.

3.3. The Effect of Volumetric Flow Rate of Liquid on HGMS

Figure 4 presents the variations of penetration P with V_{LF} at various volumetric flow rates of the liquid Q_{LF} (0.833, 0.545 and 0.417 L min^{-1}) or the liquid flow velocity v_0 (1.731, 1.132 and 0.866 m min^{-1}; = Q_{LF}/A_c, A_c = 4.8125 cm^2), with $C_{LF,i}$ = 2.06 g L^{-1}. It shows that HGMS is more quickly saturated if the Q_{LF} is higher. For v_0 = 1.731 m min^{-1}, the V_{LF} at P95 is smallest at 131.5 V_c. As for v_0 = 0.866 of m min^{-1}, the V_{LF} at P95 is largest at 191.2 V_c. At v_0 = 1.132 of m min^{-1}, the V_{LF} at P95 is 157.3 V_c. The decrease of V_{LF} at P95 with increasing Q_{LF} is due to the cause that the capture radiuses R_{ca} of the magnetic matrix become shorter as the Q_{LF} or v_0 increases, as indicated in Equation (4), resulting in a lower saturation capture capacity and quicker breakthrough and exhaustion.

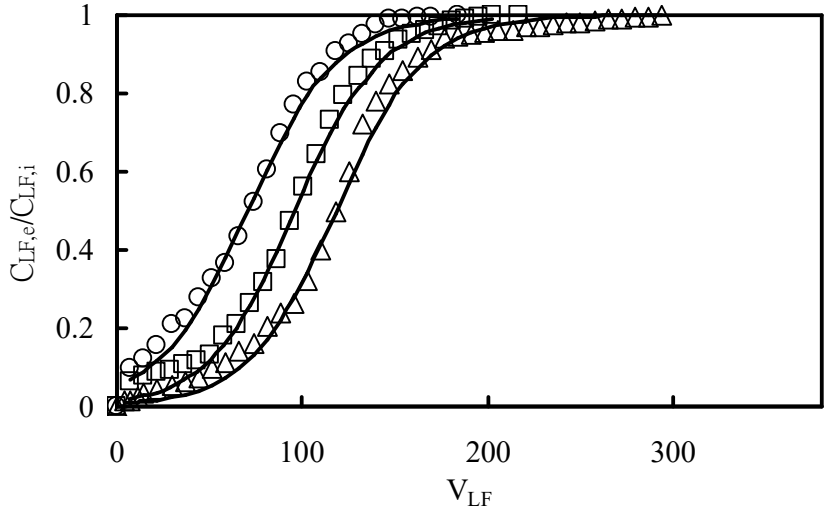

Figure 4. Breakthrough curves for the solution containing M-PVAC-IDA using HGM separator (HGF-10 1) at various Q_{LF} with $C_{LF,i}$ = 2.06 g L^{-1}. ○, □, △: Q_{LF} = 0.833, 0.545, 0.417 L min^{-1} (v_0 = 1.731, 1.132, 0.866 m min^{-1}). —: Prediction. $C_{LF,e}$, $C_{LF,i}$, V_{LF}, Q_{LF}: As specified in Figure 3.

In addition, Figure 5 depicts the relationship between the breakthrough time t_B (taken at *P*10 ($C_{LF,e}/C_{LF,i}$ = 10%)) and the reciprocal of the square of the fluid velocity ($1/v_0^2$). The results indicated that the effective separation time, i.e., t_B, is proportional to $1/v_0^2$. This implies that the operation time is proportional to $1/v_0^2$ if the separation efficiency η (= 1 − *P*) is given. A higher v_0 leads to a quicker breakthrough by a shorter t_B.

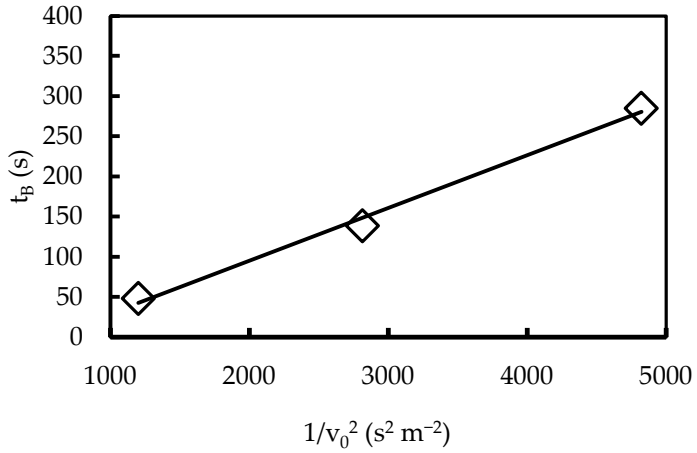

Figure 5. t_B vs. $1/v_0^2$ for the solution containing M-PVAC-IDA using HGM separator (HGF-10 1). t_B: Breakthrough time. v_0: Fluid velocity.

Figure 6 presents the variation of the saturation capture capacity (σ_S) as computed at P95 with $1/v_0$. The σ_S is proportional to $1/v_0$. It is noted that the capture capacity (σ) at $C_{LF,e}$ with V_{LF} is computed as follows.

$$\sigma = [C_{LF,i}\, V_{LF}\, V_c - \int_0^{V_{LF}\, V_c} C_{LF,e}\; d(V_{LF}\; V_c)\,]/V_c$$
$$= [C_{LF,i}\, V_{LF} - \int_0^{V_{LF}} C_{LF,e}\; d(V_{LF})\,] \quad (18)$$

In order to achieve a higher σ_S, a lower v_0 is preferred. Comparing Figures 5 and 6 further indicates that the effects of v_0 on the t_B at P10 and t_E at P95 proportional to $1/v_0^2$ are more pronounced than those on σ_S proportional to $1/v_0$. The results of Figures 5 and 6 are consistent with those of Figure 4.

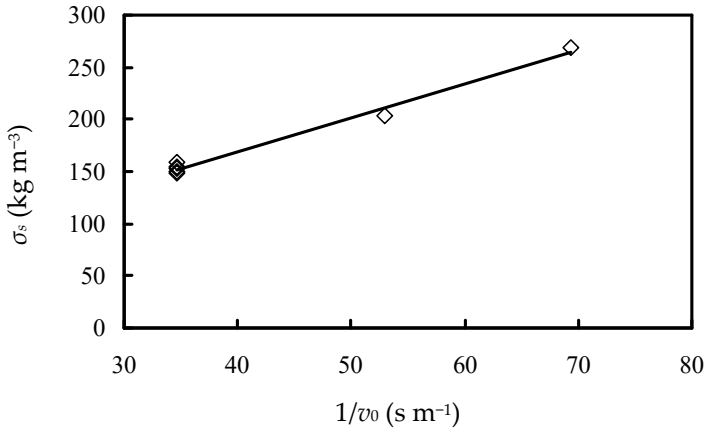

Figure 6. σ_S vs. $1/v_0$ for the solution containing M-PVAC-IDA using HGM separator (HGF-10 1). σ_S: Saturated capture capacity of HGM separator (HGF-10 1). v_0: Fluid velocity.

3.4. Modeling of the Kinetics HGMS

With σ_S, v_0 and L inserted into Equation (12) at the MPA concentrations $C_{LF,i}$ of 0.94, 1.51, 2.06, 3.21 and 4.14 g L^{-1} and the fluid velocity of 0.866, 1.132 and 1.731 m min^{-1}, the non-linear regressions were conducted. The simulated results are listed in Table 1 and plotted in Figures 3 and 4. The results show good fits with the experimental data with R^2 of 0.985–0.995.

Table 1. Parameters for prediction of the operation of high-gradient magnetic separator (HGF-10 1).

Initial Concentration	Flow Velocity	Exhaustion Time at P95	Breakthrough Time at P10	Characteristic Length	Determination Coefficient
$C_{LF,i}$	v_0	t_E	t_B	λ_0	R^2
g L^{-1}	m min^{-1} or m s^{-1}	min or s	min or s	m^{-1}	
At various $C_{LF,i}$ with Q_{LF} of 0.833 L min^{-1}					
4.14	1.731 or 0.0289	3.3 or 198	0.36 or 21.6	36.9	0.992
3.2	1.731 or 0.0289	4.4 or 264	0.53 or 31.8	37.71	0.985
2.06	1.731 or 0.0289	6.4 or 384	0.8 or 48	38.11	0.994
1.51	1.731 or 0.0289	9.3 or 558	1.7 or 102	43.65	0.986
0.94	1.731 or 0.0289	12.8 or 768	3 or 180	48.43	0.988
At various v_0 with $C_{LF,i}$ = 2.06 g L^{-1}					
2.06	1.731 or 0.0289	6.4 or 384	0.8 or 48	38.11	0.994
2.06	1.132 or 0.0189	9.8 or 588	2.31 or 138.6	53.48	0.995
2.06	0.866 or 0.0144	14.8 or 888	4.75 or 285	63.72	0.990

R^2: Determination coefficient, $= 1 - \left(\frac{[\sum(y_e - y_c)^2]}{[\sum(y_e - y_m)^2]}\right)$, where y_e and y_c, and y_m are the experimental and predicted results and the average of experimental values of $C_{LF,e}/C_{LF,i}$, respectively. $C_{LF,e}$ = outlet concentrations of MPA (M-PVAC-IDA). v_0 = 1.731, 1.132, 0.866 m min^{-1} corresponding to Q_{LF} = 0.833, 0.545, 0.417 L min^{-1}.

Taking that the $C_{LF,e}/C_{LF,i}$ = 10% represents the t_B of the separation chamber of the magnetic matrix, then the values of t_B are 3, 1.7, 0.8, 0.53 and 0.36 min at the respective concentrations of 0.94, 1.51, 2.06, 3.21 and 4.14 g L^{-1} with Q_{LF} at 0.833 L min^{-1}, and are 4.75, 2.31 and 0.8 min at respective v_0 of 0.866, 1.132 and 1.731 m min^{-1} with $C_{LF,i}$ at 2.06 g L^{-1}. These values also exhibit the same tendency with the experimental data, indicating that the higher the MPA concentration, as well as the fluid velocity, the shorter the breakthrough time. From a comparison of the initial characteristic length λ_0 for the cases with the different MPA concentrations studied, it indicates that the value of λ_0 of the kinetic models equation decreases with increasing $C_{LF,i}$. According to Equation (13), λ_0 is related to the capture radius. Thus, it can be illustrated that the higher MPA concentration has the shorter capture radius due to that MPAs block some lines of the magnetic field, causing the shorter initial characteristic length λ_0. For cases of the different flow velocities examined, it was observed that the value of λ_0 decreases as v_0 increases. It can be interpreted that the higher flow velocity has the shorter capture radius because of the larger inertial impact force, resulting in the shorter initial characteristic length.

3.5. Operation Practice

In this study, the feasibility of using HGMS as a recovery method was examined for the recycling and reuse of MPA in ADPs. In this system, the operation time of HGMS should be short, and the energy consuming should, therefore, be reduced. Thus, t_B is one of the important parameters of the magnetic separation operation. The HGMS with a short t_B indicates that the operation of the magnetic separation chamber should be better when periodic. In one cycle, the HGMS of the magnetic particles must be stopped before reaching t_B to avoid a great loss of the magnetic particles in the effluent of the separation

chamber of the HGMS. According to the results of previous sections, t_B is not only affected by the particle concentration, but also influenced by the fluid velocity. In the Watson and Gerber theory, a decrease of the R_{ca} with increasing MPA concentration or flow velocity was deduced. This was confirmed, as the t_B of the HGMS of MPA was shortened when the MPA concentration, as well as the flow velocity, increased. It was explained by the cause that the R_{ca} is influenced by drag force and magnetic force. By using the deep-bed filtration model, a good qualitative description of the results in this study was obtained. In this model, a decrease of the initial characteristic length λ_0 with an increasing MPA concentration or flow velocity was observed. In a single wire, λ_0 is directly proportional to R_{ca}, based on Equation (13). Thus, it is also attributed to fluid drag force and magnetic force. It also describes the steepness of the particle breakthrough curve. Therefore, the lower λ_0 means the HGMS has a lower recovery ability of MPA.

The flow velocity is also indeed an important factor in high-gradient magnetic separation. In order to increase the treatment volume and to shorten the treatment time in operation, what is usually done is increasing the flow velocity. However, if the flow velocity is too high, it will dramatically decrease the separation efficiency and greatly shorten the effective t_B, too. Thus, the flow velocity setting is important for high-gradient magnetic separation. Suppose that t_{ON} is the necessary operation time interval for the separation of magnetic media to facilitate the switching of the magnetic field. Equation (19) can be deduced from Equation (12) under the given separation efficiency η (or P_0) and operation time t_{ON}, yielding

$$1 - \eta = 1 - P_0 = P = C_{LF,e}/C_{LF,i} \geq [\exp(C_{LF,i}\, v_0 \lambda_0 \tau/\sigma_S)]/([\exp(C_{LF,i}\, v_0 \lambda_0 \tau/\sigma_S)] + [\exp(\lambda_0 L)] - 1) \quad (19)$$

At the conditions of the given $C_{LF,i}$ = 2.06 kg m^{-3}, η (or P_0) = 0.9 and t_{ON} = 120 s, then v_0 can be calculated from the equation to be lower than 0.01 m s^{-1}.

The lower the flow velocity, the higher the separation efficiency is. However, it has been thought that the flow velocity cannot decrease without any limitation. It must be higher than the speed of sweeping and scouring to avoid the deposit of the magnetic particles on the tube wall. As calculated from Equation (20), which, with the substitution of the friction coefficient f_c (Equation (21)), yielding Equation (22), supposing r_h = 0.005 m, ρ_p =1.629 kg cm^{-3} in Equation (22), a flow velocity above 2.47 × 10^{-3} m s^{-1} is thought to be more suitable. This means that the flow velocity must overcome the friction shearing stress caused by the gravity of the magnetic particles to avoid the deposit of magnetic particles on the tube wall, which, however, increases the particle loss of M-PVAC-IDA.

$$v_0 \geq [(8\gamma/f_c)\, g\, ((\rho_p - \rho_w)/\rho_w)\, d_p]^{0.5} \quad (20)$$

$$f_c = 64/Re = 64\mu/(\rho_w\, v_0\, 4r_h) \quad (21)$$

Equation (22) can be obtained, as Equation (20) is taken into the relationship of the friction coefficient of Equation (21).

$$v_0 \geq [(\gamma\, r_h\, g\, (\rho_p - \rho_w)/(2\mu_w))\, d_p]^{0.5} \quad (22)$$

In the above equations, r_h is the hydraulic radius, f_c is the friction coefficient, γ is the constant (0.03–0.06), ρ_p is the density of the magnetic particles, ρ_w is the density of the water, d_p is the particle diameter of the magnetic particles, Re is the Reynolds number and g is the acceleration due to gravity.

Noting the low running cost and small space requirement of the new magnetic separation system, the broad applications involving HGMS will attract more attention in the future. The information obtained in this study is useful for the rational design and proper operation of a HGMS system for the recycling and reuse of MPA in ADPs.

4. Conclusions

Through the results and discussion elucidated above, we can draw the following essential conclusions.

1. Due to fact that the capture radius of a HGM separator is inversely proportional to the inlet concentration of MPA ($C_{LF,i}$), the higher concentration of M-PVAC-IDA leads to the shorter breakthrough time (t_B). The higher volumetric flow rate (Q_{LF}) also results in the shorter t_B.
2. The saturation capture capacity (σ_S) is inversely proportional to the flow velocity (v_0); the breakthrough time is inversely proportional to the square of the flow velocity.
3. If $C_{LF,i}$ = 2.06 kg m^{-3}, the separation efficiency η = 0.9 and the operation time t_{ON} = 120 s, then v_0 can be calculated from the kinetic equation to be lower than 0.01 m s^{-1}. The flow velocity exceeding 2.47 × 10^{-3} m s^{-1} is considered more proper in order to prevent the deposit of the magnetic particles on the tube wall.
4. The experimental data show a good fit with the mass balance approach model equation with a R^2 of 0.985–0.995.
5. The value of the characteristic length (λ_0) of the kinetic model equation decreases with an increasing flow velocity.

Author Contributions: Conceptualization, J.-Y.T. and C.-Y.C.; methodology, J.-Y.T. and C.-Y.C.; validation, C.-W.T., D.-R.J. and B.-L.L.; formal analysis, J.-Y.T. and C.-W.T.; verification, J.-Y.T. and C.-Y.C.; discussion, suggestions and resources, C.-Y.C., C.-C.C., C.-F.C., Y.-H.C., J.-L.S., M.-H.Y. and M.F.; writing—original draft preparation, J.-Y.T. and C.-Y.C.; writing—review and editing, M.-H.Y. and C.-Y.C.; supervision, C.-Y.C.; funding acquisition, M.-H.Y. and C.-Y.C. All authors have read and agreed to the published version of the manuscript.

Funding: This research was funded by the National Science and Technology Council of Taiwan (formerly National Science Council), NSC 97-2221-E-002-113-MY3 and NSTC 111-2622-E-039-001.

Data Availability Statement: Data sharing not applicable.

Conflicts of Interest: The authors declare no conflict of interest.

Nomenclature

A_c	Cross section area of filter or separation cell, cm^2 or m^2; = 4.8125 cm^2 in this study
A_1	Defined in Equation (5), cm or m
A_2	Defined in Equation (16), cm^{-1} or m^{-1}
a	Radius of ferromagnetic wire of matrix, cm or m; placed axially along z axis
a_B	Radius of particle buildup profile (actual wire radius of magnetic media with build up of particles), m
B	Magnetic flux density, or magnetic induction, G; B(G) = $\mu_0 H$ (Oe)
C	Concentrations of MPA (i.e., M-PVAC-IDA) in solution, mg L^{-1} or g L^{-1}
$C_{LF,i}$, $C_{LF,e}$	Inlet and outlet concentrations of MPA (i.e., M-PVAC-IDA) in solution, mg L^{-1} or g L^{-1}
dx	Differential thickness of filter, m
d_p	Diameter of paramagnetic particle, μm or nm
F	Filling factor (or filling density) of matrix, -; = $L_{wx}\,\pi a^2/(dx\,A_c)$ or $L_{wm}\,\pi a^2/(\mathrm{L}\,A_c)$ (= V_{wm}/V_c = 4.37/37.78 = 0.1157 filled with all matrix of 34.5466 g received in this study)
F_c	Limiting F, -; if wires in filter are separated by a distance greater than $2X_c$, than particles interact with only one wire at a time, i.e., wires act independently; $\sim 3\pi/(4X_c^2)$ [35]
F_d	Viscous resistance force (viscous drag force), N
F_m	Magnetic force, N
$F_{m/v}$	Magnetic force per unit volume, N m^{-3}
f	Matrix arrangement factor in Equation (1), -
f_c	Friction coefficient in Equation (21), -
g	Acceleration due to gravity

H	Magnetic field strength, or magnetic field intensity, Oe; applied in x direction
H_0	H applied in x direction perpendicular to filter, Oe
∇H	Magnetic field strength gradient at the location of particle; i.e., grad(H)
L	Height of separation chamber housing magnetic filter media, m or cm; = 7.85 cm in this study
L_{AT}	Adsorption treated liquid
L_a	Normalized L, -; = L/a
L_{RF}	Fresh liquid for regeneration of aged magnetite
L_{RA}	Aged regeneration liquid (liquid after regeneration of aged magnetite)
L_{WL}	Waste liquid
L_{wm}	Length of wire of matrix, m
L_{wx}	L_{wm} in a thickness dx of filter, m; $L_{wx}/A_c = Fdx/(\pi a^2)$
L_{wxe}	Effective L_{wx}, m; = (2/3)L_{wx}, assuming approximately 1/3 of L_{wx} is parallel to H_0 and ineffective in filtering process [35]
M	Magnetization, emu g^{-1} or emu cm^{-3}
M_A	Atomic mass
M_{ad}	Molecular weight of adsorbate
M_{MA}	Aged magnetite
M_{MF}	Fresh or freshed (regenerated) magnetite
M_p	Magnetization of particles, emu g^{-1} or emu cm^{-3} or A m^2 cm^{-3}; = $(\chi_p - \chi_f)\,H$
M_{pS}	Saturation magnetization of magnetic particles, emu g^{-1}
M_r	Residual magnetization, emu g^{-1}
M_S	Saturation magnetization, emu g^{-1}
M_{Sp}	M_S of particles, emu g^{-1}
M_{wm}	Magnetization of wire of matrix, emu g^{-1} or emu cm^{-3}
m_{wm}	Mass of wire of matrix, g or kg; = 34.5466 g for all matrix as received in this study
N_i	Number of particles per unit volume of incident on filter, m^{-3}
N_e	Number of particles per unit volume of outlet fluid from filter, m^{-3}; = $N_i \exp(-4FR_{ca}L/(3\pi a))$ for cases (1) in streamline flow with a filling factor less than F_c, and (2) in the limit of extreme turbulent [35]
P	Penetration of magnetic particles in fluid, -; = $C_{LF,e}/C_{LF,i} = 1 - \eta$
P_0 or η	Separation efficiency, -; = $1 - P$
$P10$	P = 10%
$P95$	P = 95%
Q_{LF}	Volumetric flow rate of liquid, L min^{-1}
R_{ca}	Dimensionless normalized particle capture radius, -; = r_c/a; if position of particle with initial coordinate $(y/a)_i$ for large x/a satisfies $R_{ca} \geqq (y/a)_i \leqq -R_{ca}$, then the particle will be captured; $R_{ca} \sim (1/2)v_m/v_0$ for small values of v_m/v_0 (say, $\leqq$ 1), however $R_{ca} \sim (1/4)v_m/v_0$ for v_m/v_0 =10 [35]
Re	Reynolds number, -; = $\rho_w v_0 4r_h/\mu_w$
R^2	Determination coefficient
r	Radius of circular pipe, m
r_c	Particle capture radius, m
r_h	Hydraulic radius, m; = ratio of cross-section area/wetted perimeter (= $\pi r^2/(2\pi r)$ = $r/2$ for circular pipe)
r_p	Radius of paramagnetic particle, μm or nm
t	Filtration time (also called separation time or operation time), s
t_B	Breakthrough time (or effective separation time) for HGMS, s; estimated as at P = $C_{LF,e}/C_{LF,i}$ = 10%
t_E	Exhaustion time (or saturation time) for HGMS, s; estimated as at P = $C_{LF,e}/C_{LF,i}$ = 95%
t_{ON}	Necessary operation time interval for separation of magnetic media to facilitate the switching of magnetic field, s
t_η	Separation time at a set separation efficiency η (= 1 − P) for HGMS, s
V_c or CV	Volume of filter chamber or cell volume, cm^3 or m^3; = 37.78 cm^3 in this study
V_{LF}	Accumulated volume of liquid filtrated expressed as CV
V_p	Volume of a magnetic particle (= (4/3) π r_p^3 for spherical particle), nm^3

V_{wm}	Volume of wire of matrix, cm^3 or m^3; = m_{wm}/Q_{wm} = 34.5466 g/7900 (kg/m^3) = 0.00000437 m^3 for all matrix as received in this study
v	Velocity, m s^{-1}
v_m	Characteristic magnetic velocity, m s^{-1}
$v_{p/f}$	Velocity of magnetic particle relative to fluid, m s^{-1}
v_0	Fluid velocity (superficial velocity), m s^{-1}; the magnetic wire is placed axially along z axis with the uniform magnetic field strength applied in x direction while fluid flowing past the wire in negative x direction.
X	x/a, -
X_c	Dimensionless distance from wire at which particle has changed y/a coordinate by 5% from initial value of $(y/a)_i$, - [35]
x, y, z	x, y and z directions of rectangular coordinates
Y	y/a, -
$(y/a)_i$	Initial coordinate of position of particle
β	Packing factor of the buildup (i.e., particle aggregation factor), -; = 0.1-0.18
γ	Constantin in Equation (20), -; = 0.03-0.06
ε_F	Filter void fraction, (-); = $(V_c - V_{wm})/V_c = 1 - F$ (= 0.8843 with all received matrix of 34.5466 g filled in the chamber)
η or P_0	Separation efficiency of MP for HGMS, -; = $1 - P$
λ	Characteristic length, m^{-1}; = $\lambda_0 [1 - (\sigma/\sigma_S)]$
λ_0	Characteristic length at $\tau = 0$, m^{-1}; = $(2/\pi)(1 - \varepsilon_F)(R_{ca}/a)$
μ_f	Viscosity of fluid, kg $m^{-1}s^{-1}$ or N s m^{-2}
μ_r	Magnetic permeability of medium relative to that of vacuum, -, $= \mu'/\mu_0$
μ_w	Viscosity of water, kg $m^{-1}s^{-1}$ or N s m^{-2}
μ_0	Magnetic permeability of vacuum, H m^{-1}, = $4\pi \times 10^{-7}$ H m^{-1}
μ'	Magnetic permeability, H m^{-1}
ρ_p	Density of magnetic particles, kg m^{-3}
ρ_w	Density of water, kg m^{-3}
ρ_{wm}	Density of wire of matrix, g/cm^3 or kg/m^3; = 7900 kg/m^3 in this study
σ	Capture capacity of magnetic particle on the magnetic media in magnetic separation cell at time t, kg m^{-3}
σ_S	Saturated σ, kg m^{-3}
σ_{Ei}	Surface charge density of layer with ions i
τ	Time defined by $\tau = t - (\varepsilon_F x/v_0)$, s
χ	Magnetic susceptibility, emu cm^{-3} Oe^{-1} ;= Mp/H
χ_p	Magnetic susceptibility of particle, emu cm^{-3} Oe^{-1}
χ_f	Magnetic susceptibility of fluid, emu cm^{-3} Oe^{-1}
Subscripts	
f	Fluid
p	Particle
Abbreviations	
A-MPAs	Exhausted adsorbed MPAs
ADPs	Adsorption and desorption processes
CV	Cell volume
D-MPAs	Fresh or Regenerated desorbed MPAs
DW	Dry weight
HGMS	High-gradient magnetic separation
IDA	Iminodiacetic acid
NdFeB	Neodymium-iron-boron
M-PVA-IDA	MPA of polyvinyl acetate-iminodiacetic acid
MPA	Magnetic polymer adsorbent or super-paramagnetic polymer adsorbent
MS	Magnetic separation
OD	Optical density
PVA	Polyvinyl acetate
VAC	Vinyl acetate

Appendix A

The solution of the outlet concentration $C_{LF,e}$ (Equation (12)) was obtained as follows:

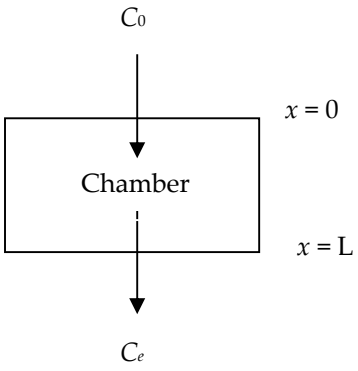

Figure A1. Sketch of mass balance approach for kinetic models of HGMS.

$$\frac{\partial \sigma}{\partial \tau} + V_0 \frac{\partial C}{\partial x} = 0 \tag{A1}$$

$$\frac{\partial \sigma}{\partial \tau} = \lambda V_0 C \tag{A2}$$

$$\lambda = \lambda_0 \left(1 - \frac{\sigma}{\sigma_S} \right) \tag{A3}$$

$$\tau = t - \frac{\varepsilon_F x}{V_0} \tag{A4}$$

with the conditions:

$$x = 0,\ C = C_0 \tag{A5}$$

$$\tau = 0,\ \sigma = 0 \tag{A6}$$

Combining Equations (A1)–(A3) gives

$$\frac{\partial \sigma}{\partial \tau} = -V_0 \frac{\partial C}{\partial x} = \lambda_0 \left(1 - \frac{\sigma}{\sigma_S} \right) V_0 C \tag{A7}$$

$$-\frac{dC}{C} = \left(\lambda_0 - \frac{\sigma \lambda_0}{\sigma_S} \right) dx \tag{A8}$$

$$\frac{dC}{C} = \left(\frac{\sigma \lambda_0}{\sigma_S} - \lambda_0 \right) dx \tag{A9}$$

Integration of Equation (A9) leads to

$$\ln C = \frac{\lambda_0}{\sigma_s} \int_0^x \sigma dx - \lambda_0 x + k(\tau) \tag{A10}$$

Appling condition ($x = 0$, $C = C_0$) gives $\ln C_0 = k(\tau)$. Then, Equation (A10) becomes

$$\ln\frac{C}{C_0} = \sigma' - \lambda_0 x \quad \text{with} \quad \sigma' = \frac{\lambda_0}{\sigma_S}\int_0^x \sigma dx \tag{A11}$$

Substituting condition $\tau = 0$, $\sigma = 0$ gives

$$\ln\frac{C}{C_0} = -\lambda_0 x \tag{A12}$$

Equation (A11) can be partially differentiated by τ. This leads to

$$\frac{1}{C}\frac{dC}{d\tau} = \frac{\lambda_0}{\sigma_S}\int_0^x \frac{\partial\sigma}{\partial\tau}dx \tag{A13}$$

Substitution of $\frac{\partial\sigma}{\partial\tau}$ by $-V_0\frac{\partial C}{\partial x}$ from Equation (A2) results in

$$\frac{1}{C}\frac{dC}{d\tau} = \frac{\lambda_0}{\sigma_S}\int_0^x -V_0\frac{\partial C}{\partial x}dx = -\frac{\lambda_0 V_0}{\sigma_S}\int_{C_0}^{C} dC = -\frac{\lambda_0 V_0}{\sigma_S}(C - C_0) \tag{A14}$$

Integrating Equation (A14) leads to

$$\frac{C}{C_0} = \frac{[\exp(A)]\,U(x)}{([\exp(A)]\,U(x)) - 1} \tag{A15}$$

where

$$\mathrm{A} = \frac{\lambda_0 \mathrm{V}_0 \mathrm{C}_0}{\sigma_\mathrm{S}}\tau \tag{A16}$$

At $\tau = 0$, Equation (A15) gives

$$\left.\frac{C}{C_0}\right|_{\tau=0} = \frac{U(x)}{U(x) - 1} \tag{A17}$$

Comparison of Equations (A12) and (A17) leads to

$$\left.\frac{C}{C_0}\right|_{\tau=0} = \exp(-\lambda_0 x) = \frac{U(x)}{U(x) - 1} \tag{A18}$$

Then

$$U(x) = \frac{\exp(-\lambda_0 x)}{\exp(-\lambda_0 x) - 1} \tag{A19}$$

Equation (A15) is divided by $U(x)$ to give

$$\frac{C}{C_0} = \frac{\exp(A)}{[\exp(A)] - U^{-1}(x)} \tag{A20}$$

where A is defined by Equation (A16) and

$$U^{-1}(x) = \frac{[\exp(-\lambda_0 x)] - 1}{\exp(-\lambda_0 x)} = 1 - \exp(\lambda_0 x) \tag{A21}$$

Thus

$$\frac{C}{C_0} = \frac{\exp(A)}{\exp(A) + \exp(\lambda_0 x) - 1} = \frac{\exp(\sigma_S^{-1}\lambda_0 C_0 V_0 \tau)}{\exp(\sigma_S^{-1}\lambda_0 C_0 V_0 \tau) + \exp(\lambda_0 Z) - 1} \tag{A22}$$

The outlet concentration C at $x = L$ is then obtained as

$$\frac{C}{C_0}\Big|_{x=L} = \frac{\exp(\sigma_S^{-1}\lambda_0 C_0 V_0 \tau)}{\exp(\sigma_S^{-1}\lambda_0 V_0 C_0 \tau) + \exp(\lambda_0 L) - 1} \tag{A23}$$

References

1. Richard, G.; Robert, R.B. *High Gradient Magnetic Separation*; Department of Pure and Applied Physics, University of Salford: Salford, UK, 1983.
2. Lofthous, C. The beneficiation of kaolin using a commercial high intensity magnetic separator. *IEEE Trans. Magn.* **1981**, *17*, 3302–3304.
3. Trindade, S.C. Studies on the Magnetic Demineralization of Coal. Ph.D. Dissertation, Massachusetts Institute of Technology, Cambridge, MA, USA, 1973.
4. Mizuki, T.; Watanabe, N.; Nagaoka, Y.; Fukushima, T.; Morimoto, H.; Usami, R.; Maekawa, T. Activity of an enzyme immobilized on superparamagnetic particles in a rotational magnetic field. *Biochem. Biophys. Res. Commun.* **2010**, *393*, 779–782.
5. Rotariu, O.; Strachan, N.J.C. Modelling magnetic carrier particle targeting in the tumor microvasculature for cancer treatment. *J. Magn. Magn. Mater.* **2005**, *293*, 639–646.
6. Furlani, E.J.; Furlani, E.P. A model for predicting magnetic targeting of multifunctional particles in the microvasculature. *J. Magn. Magn. Mater.* **2007**, *312*, 187–193.
7. Epherre, R.; Goglio, G.; Mornet, S.; Duguet, E. Hybrid magnetic nanoparticles for targeted delivery. In *Comprehensive Biomaterials*; Ducheyne, P., Healy, K.E., Grainger, D.W., Hutmacher, D.W., Kirkpatrick, C.J., Eds.; Elsevier: Waltham, MA, USA, 2011; Volume 4, pp. 575–593.
8. Franzreb, M.; Siemann-Herzberg, M.; Hobley, T.J.; Thomas, O.R.T. Protein purification using magnetic adsorbent particles. *Appl. Microbial. Biot.* **2006**, *70*, 505–516.
9. Meyer, A.; Berensmeier, S.; Franzreb, M. Direct Capture of lactoferrin from whey using magnetic micro-ion exchangers in combination with high-gradient magnetic separation. *React. Funct. Polym.* **2007**, *67*, 1577–1588.
10. Chalmers, J.J.; Zborowski, M.; Sun, L.P.; Moore, L. Flow through, immunomagnetic cell separation. *Biotechnol. Progr.* **1998**, *14*, 141–148.
11. Tokoro, H.; Nakabayashi, T.; Fujii, S.; Zhao, H.; Hafeli, U.O. Magnetic iron particles with high magnetization useful for immunoassay. *J. Magn. Magn. Mater.* **2009**, *321*, 1676–1678.
12. Baksheeva, I.I.; Burdakova, E.A.; Rostovtsev, V.I.; Plotnikova, A.A.; Zhizhaev, A.M.; Bondarenko, G.N. Improvement of processing of gold-bearing sulfide minerals by treatment by magnetic colloids. *J. Min. Sci.* **2022**, *58*, 135–143.
13. Chan, M.Y.; Lee, Y.K.; Yeap, S.P. pH-dependent adsorption/desorption of dye molecules using magnetically separable quartz sand. *J. Teknol.* **2022**, *84*, 1–8.
14. Okumura, M.; Akiyama, Y.; Mori, T.; Okada, H.; Hirota, N.; Yamaji, T.; Matsuura, H.; Namba, S.; Sekine, T.; Mishima, F.; et al. Removal of iron oxide scale from boiler feed-water in thermal power plant by magnetic separation-scale removal at high-temperature. *IEEE Trans. Appl. Supercond.* **2022**, *32*, 3700705.
15. Wang, Z.; Li, X.; Wang, Z.; Huang, W.; Liy, G.; Zeng, C.; Huang, L. Separation of copper-molybdenum flotation concentrate by superconducting high-gradient magnetic separation. *Minerals* **2022**, *12*, 1191.
16. Zheng, X.; Jing, Z.; Sun, Z.; Liu, D.; Yasi, G.; Wang, Y. Significantly improved separation efficiency of refractory weakly magnetic minerals by pulsating high-gradient magnetic separation coupling with magnetic fluid. *ACS Sustain. Chem. Eng.* **2022**, *10*, 10105–10118.
17. Tseng, J.Y.; Chang, C.Y.; Chen, Y.H.; Chang, C.F.; Chiang, P.C. Synthesis of micro-size magnetic polymer adsorbent and its application for the removal of Cu(II) ion. *Colloids Surf. A Physicochem. Eng. Asp.* **2007**, *295*, 209–216.
18. Tseng, J.Y.; Chang, C.Y.; Chang, C.F.; Chen, Y.H.; Chang, C.C.; Ji, D.R.; Chiu, C.Y.; Chiang, P.C. Kinetics and equilibrium of desorption removal of copper from magnetic polymer adsorbent. *J. Hazard. Mater.* **2009**, *171*, 370–377.
19. Mariani, G.; Fabbri, M.; Negrini, F.; Ribani, P.L. High-gradient magnetic separation of pollutant from wastewaters using permanent magnets. *Sep. Purif. Technol.* **2010**, *72*, 147–155.
20. Khan, Z.H.; Gao, M.; Giu, W.; Qaswar, M.; Islam, M.S.; Song, Z. The sorbed mechanisms of engineering magnetic biochar composites on arsenic in aqueous solution. *Environ. Sci. Pollut. Res.* **2020**, *27*, 41361–41371.

21. Chen, H.; Miura, O. Removal of magnetic fine particles from carbon black powder by high gradient magnetic separation under dry condition. *IEEE Trans. Appl. Supercond.* **2022**, *32*, 3700605.
22. Hu, Z.; Liu, J.; Can, T.; Lu, D.; Wang, Y.; Zheng, X. High-intensity magnetic separation for recovery of $LiFePO_4$ and graphite from spent lithium-ion batteries. *Sep. Purif. Technol.* **2022**, *297*, 121486.
23. Jiang, Y.; Chen, L.; Duan, S.; Gao, Q.; Yi, F.; Xian, Y. Deep insight on the occurrence feature of iron minerals in a cyanide leaching residue and its effective recovery with magnetic separation. *Minerals* **2022**, *12*, 524.
24. Ramage, S.J.F.F.; Pagaling, E.; Haghi, R.K.; Dawson, L.A.; Yates, K.; Prabhu, R.; Hillier, S.; Devalla, S. Rapid extraction of high- and low-density microplastics from soil using high-gradient magnetic separation. *Sci. Total Environ.* **2022**, *831*, 154912.
25. Li, M.K.; Kessler, J.; Bach, D.T. Magnetic Separation Device and Methods for Use in Heterogeneous Assays. U.S. Patent 4,988,618, 29 January 1991.
26. Liberti, P.A.; Wang, Y.Z.; Tang, W.X.; Feeley, B.P.; Gohel, D.I. Apparatus and Methods for Magnetic Separation Featuring External Magnetic Means. U.S. Patent 5,466,574, 14 November 1995.
27. Zborowski, M.; Fuh, C.B.; Green, R.; Sun, L.P.; Chalmers, J.J. Analytical magnetapheresis of ferritin-labeled lymphocytes. *Anal. Chem.* **1995**, *67*, 3702–3712.
28. Blankenstein, G. *Microfabricated Flow System for Magnetic Cell and Particle Separation in Scientific and Clinical Applications of Magnetic Carriers*; Plenum Press: New York, NY, USA, 1997.
29. Watson, J.H.P. High gradient magnetic separation. In *Solid-Liquid Separation*, 3rd Ed.; Svarovsky, L., Ed.; Butterworth-Heinemann: Oxford, UK, 1990.
30. Dauer, R.R.; Dunlop, E.H. High gradient magnetic separation of yeast. *Biotechnol. Bioeng.* **1991**, *37*, 1021–1028.
31. Richards, A.J.; Lansdorp, P.M. Magnetic Filter with Ordered Wire Array. U.S. Patent 5,439,586, 8 August 1995.
32. Miltenyi, S. Magnetic Separation Apparatus. U.S. Patent 5,711,871, 27 January 1998.
33. Burns, M.A.; Graves, D.J. Application of magnetically stabilized fluidized beds to bioseperations. *React. Polym.* **1987**, *6*, 45–50.
34. Goto, M.; Imamura, T.; Hirose, T. Axial dispersion in liquid magnetically stabilized fluidized beds. *J. Chromatogr. A* **1995**, *690*, 1–8.
35. Watson, J.H.P. Magnetic filtration. *J. Appl. Phys.* **1973**, *44*, 4209–4213.
36. Gerber, R.; Lawson, P. The HGMS filter performance experimental law. *IEEE Trans. Magn.* **1989**, *25*, 3806–3808.
37. Ebner, A.D.; Ritter, J.A. Concentrating dilute sludge wastes with high-gradient magnetic separation: Breakthrough experiments and performance. *Ind. Eng. Chem. Res.* **2002**, *41*, 5049–5057.
38. Qi, Z.; Joshi, T.P.; Liu, R.; Li, Y.; Liu, H.; Qu, J. Adsorption combined with superconducting high gradient magnetic separation technique used for removal of arsenic and antimony. *J. Hazard. Mater.* **2018**, *343*, 36–48.